GALAXY NUCLEAR VARIABILITY AS A PROBE OF AGN STRUCTURE

by

Adam K. Johanson

A senior thesis submitted to the faculty of

Brigham Young University

in partial fulfillment of the requirements for the degree of

Bachelor of Science

Department of Physics and Astronomy

Brigham Young University

April 2007

BRIGHAM YOUNG UNIVERSITY

DEPARTMENT APPROVAL

of a senior thesis submitted by

Adam K. Johanson

This thesis has been reviewed by the research advisor, research coordinator, and department chair and has been found to be satisfactory.

Date	J. Ward Moody, Advisor
Date	Eric Hintz, Research Coordinator
Date	Scott Sommerfeldt, Department Chair

ABSTRACT

GALAXY NUCLEAR VARIABILITY AS A PROBE OF AGN STRUCTURE

Adam K. Johanson

Department of Physics and Astronomy

Senior Thesis

Active galactic nucleus or "AGN" refers to any galactic nucleus that emits non-thermal radiation. Arguments based on energy requirements, light travel times, and limited observational imaging data strongly suggest that the radiation is coming from a supermassive black hole surrounded by an accretion disk. Details of the accretion disk and its surrounding material are only known in theory since no disk is close enough or unobscured enough to be imaged. The only direct probe of the disk environment comes from looking at how energy from flares in the disk "reverberate" through the surrounding gas clouds and re-emerge as emission lines. We are laying the foundation of a long-term multi year campaign of reverberation mapping by measuring the nuclear flaring or variability of the nearby edge on normal galaxies M81 and M101. We report on aperture photometry on these galaxy nuclei, compared with reported reference stars.

ACKNOWLEDGMENTS

I would like to acknowledge Eric C. Allan, who worked along with me side by side and gave me the needed encouragement to make this project possible. I would also like to acknowledge my advisor, Dr. Moody, for giving advice and guiding my efforts.

I would also like to thank Tenagra Observatories for the use of their telescope time and for the data.

Finally, I would like to dedicate this to my dear wife, Elizabeth, and my daughter, Megan. I want to thank them for their patience and support as I spent many long hours away from them working on this thesis.

Contents

List of Tables

List of Figures

Chapter 1

Introduction and Background

1.1 Active Galactic Nuclei

Like our own Milky Way, galaxies spread throughout the universe are home to billions and billions of stars. From Earth, observations of outside galaxies reveal that most of these stars are located around a central nucleus, with a decreasing concentration towards the outer rims. For the most part, the light which is seen from these galaxies are due to the starlight from its numerous members. Occasionally, there will be a galaxy with a small core within the nucleus that will put out more electromagnetic radiation than the rest of the galaxy combined. Spectroscopic analysis of these nuclei show features that cannot be attributed to starlight. Such a galaxy is termed an active galactic nucleus.

The current standard model (Carrol et al. 1996) for active galactic nuclei (AGNs) predicts a supermassive black hole at the center. Strong gravitational forces attract nearby material which flows into a surrounding accretion disk. Surrounding this accretion disk exists varying amounts of obscuring gas and dust. AGNs are classified into three main classes, quasars, radio galaxies, and blasars. As the research of these classes developed, a unified model was developed and showed that the primary difference between the three types of AGNs was the angle at which the galaxy was oriented to the observer. It was determined that all three classes were manifestations of the same object.

1.1.1 Seyfert Galaxies

AGNs were initially discovered by Carl Seyfert, after whom particular AGNs were named. Seyfert galaxies have spectra revealing emission line that have been significantly broadened through Doppler effects. (Carrol et al. 1996) The material in

the accretion disk is spinning violently due to the intense gravitational forces. Another important aspect of Seyfert galaxies is the rate of variation in their luminosity. This variation not only gives astronomers information about its size, but also about the physics involved at the center.

Synchrotron Radiation

One of the indicators that a supermassive black hole exists at the center of our object, is the overwhelming emission of synchrotron radiation. Synchrotron radiation occurs when charged particles (usually electrons in our case) are accelerated. Charged particles accelerate in magnetic fields, which are very strong around the accretion disk. Electric charges move according to the Lorentz force law,

$$F = q(v \times B) \tag{1.1}$$

Any perpendicular motion to the magnetic field lines causes an inward force that drives the particle in circular motion. Any parallel motion to the magnetic field lines doesn't accelerate the particle. In general, electrons helix around the magnetic field lines, and synchrotron radiation is observed when the velocity is parallel to the observer. The faster the electrons move, the higher the frequency of radiation.

Quasars

When Quasars were initially discovered, they were fist discovered as radio sources. Later, their optical counterparts were discovered and appeared to be ordinary stars. Further analysis revealed that these "stars" had emission lines similar to Seyfert galaxies. Eventually, doppler redshift analysis on these objects revealed that they were located at enormous distances, with the nearest one being 250 Mpcs distant. (Freedman et al. 2005) It was soon concluded that they obviously were not stars, but extremely distant galaxy nuclei.

Radio Lobed

AGNs viewed edge-on are seen as double-lobed radio galaxies. Large amounts of gas are expelled from the nucleus, often extending to distances greater than the hosting galaxy. The cause of these tremendous radio lobes is the immense synchrotron radiation being expelled from the nucleus. The speeds at which the charged particles are traveling carry so much momentum that it pushes the surrounding gas out beyond the extent of the galaxy.

Blasars

Blasars are a third type of AGN, viewed directly on the pole where the energetic jets streaming from the supermassive black holes. The jets outshine the rest of the galaxy, and once again, synchrotron radiation indicates very strong gravitational forces at work.

1.1.2 Significance

Recent studies have suggested that all galaxies have black holes in their nuclei. (Van der Marel 1999) In other words, all galaxies have the same source at their core driving the same physics. If this were true, then all galaxy nuclei would be active in some degree or another. In at least some small degree, all galactic nuclei should exhibit the same physical behavior. Obviously, the amount of energy emitted would depend directly upon the mass or strength of the black hole at the center. For the current AGN model, estimated masses for the black holes are as much as a billion solar masses. This is certainly not the case for all galaxies. However, if a black hole were at the center of every galaxy, then similar effects would take place, but on a smaller scale. As previously mentioned with Seyfert galaxies, there is significant luminosity variation. There should be similar variation in normal galaxies, but at much lower magnitude differences and different timescales.

1.1.3 New Procedure

We are laying foundations for testing a new analysis procedure, in order to detect optical variations accurate down to the milimagnitude level. Typical previous observations used stable foreground stars within the frame as references. Here we present a few stars that could be used as standard comparison stars. It has been proposed (McNeil 2004) that greater accuracy could be obtained by comparing variability with reference to the nuclear bulge. Since the bulge radiation is overwhelmingly due to stable starlight, the brightness profile should be constant down to the millimagnitude level.

With differential aperture photometry already completed on the nucleus, further research comparing the bulge profiles to the typical standard stars will give credibility to this new approach. Success in the new procedure would lay a foundation for AGN and other galactic photometric studies, yielding an increased accuracy to previously obtained results. It will also give experimental evidence for the theory of the existence of black holes at the center of virtually all galaxies. These studies will provide the starting point for a several decade long study on galaxy nuclei, the results of which will constrain and modify contemporary models of AGNs, black holes, and galactic evolution.

Chapter 2

Observations

2.1 Tenagra

The images were taken at Tenagra Observatories in the middle of the Sonora desert in southern Arizona on the 0.81 meter telescope (fig 2.1). Seeing conditions were excellent, with often humidities in the single digits and seeing with a $2''$ FWHM. Tenagra Observatories has a 100 %, fully automated system. Because of the excellent observing conditions and the automated system, Tenagra is a popular site for observing time requests from universities. The dome automatically opens at sundown and begins taking calibration frames. Then it proceeds to take images of objects it has programmed to take throughout the night. The Tenagra telescope will also periodically automatically check the weather conditions for cloudiness, humidity, and other conditions. If rain, severe wind, or any other dangerous conditions are detected, Tenagra closes the dome and immediately shuts down. (Schwartz 2007)

Tenagra frames were taken with a SITe 1024 x 1024 CCD in the Johnson R and V filters. The plate scale is approximately $0.87''$ per pixel, and the field of view is $14.8'$ x $14.8'$. This 0.81 meter reflecting telescope has a limiting magnitude of 22 with a five minute exposure.

The table below shows the observed night and filter for each galaxy.

Galaxy	Filters	Date	Galaxy	Filters	Date
M101	B,V,R	Dec 25 2006	M81	B,V,R	Dec 01 2006
	B,V,R	Dec 26		B,V,R	Dec 02
	B,V	Jan 02 2007		B,V,R	Dec 21
	B,V	Jan 03		B,V,R	Dec 22
	B	Jan 06		B,V,R	Dec 25
	B,V	Jan 17		B,V,R	Dec 26
	B,V,R	Jan 10		B,V,R	Jan 02 2007
	B,V,R	Mar 03		B,V,R	Jan 03
	B,V,R	Mar 04		B,V,R	Jan 06
	B,V,R	Mar 07		B,V,R	Jan 07
	B,V,R	Mar 11		B,V,R	Jan 10
	B,V,R	Mar 12		B,V,R	Jan 14
	B,V,R	Mar 15		B,V,R	Mar 15
	B,V,R	Mar 16		B,V,R	Mar 16

Figure 2.1: Tenagra II telescope. Source:www.tenagraobservatories.com

Chapter 3

Data

3.1 Data Reduction

In order to detect the low amplitude variations of the galactic nucleus, we must be meticulous about the method by which we calibrate the data for analysis. Standard aperture photometry introduces errors too large for some purposes, but for our purposes we were able to obtain accurate enough results. We discuss our methods of reduction in order to increase our accuracy of results.

3.1.1 IRAF

Data reduction was completed using Image Reduction and Analysis Facility (IRAF) software (see fig 3.1). IRAF was developed by astronomers at the National Optical Astronomy Observatory for the purpose of analyzing astronomical data, especially taken from CCD arrays. We used IRAF to process our frames in order to remove unwanted effects that make the data difficult to use. We also used IRAF to do aperture photometry on the galaxy frames.

3.1.2 Raw Frames

Raw frames are the object images taken with the CCD, subject to all imperfections of earth-based telescope observing. This includes imperfections in the CCD, which cause extra electrons to flow into some of the pixels, giving these pixels extra intensity that is not characteristic of the image. Other conditions that affect images are atmospheric seeing, light pollution, and cosmic rays. A set of calibration frames called zeros, darks, and flats, are used to remove these extra pixels and impurities of the CCD. We discuss the properties of these calibration frames and the methods by which we use them to correct our image frames.

Figure 3.1: IRAF

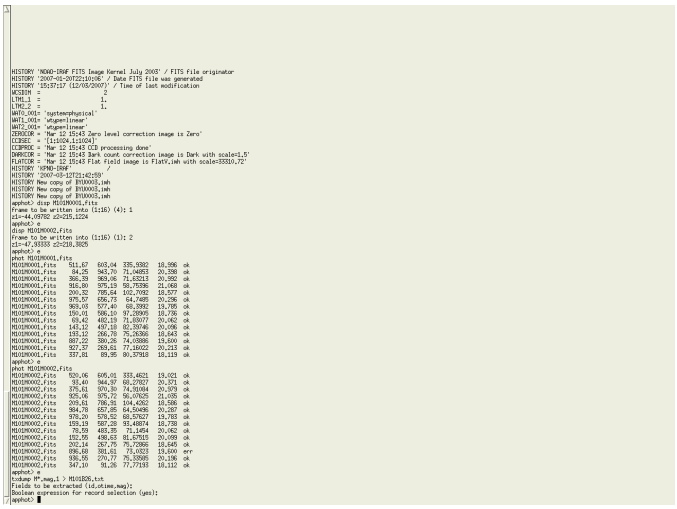

Zero

A zero or bias frame is an image taken off from a CCD that is not exposing. In essence, it reads whatever residual electrons are in the wells before even taking an image. Figure 3.2 shows such a zero frame. A perfectly good CCD would have no patters or gradients on it (Massey et al. 1992). From the Tenagra CCD, it is easily apparent that a significant gradient exists from the lower left corner to the upper right corner. This is primarily due to the way the computer reads the pixels off the CCD, starting at the lower right hand corner and finishing at the upper right. Thus, the upper right hand corner has had more time to pick up extra pixels due to the camera just being on, not even exposing. This gradient then manifests itself in all of the object frames.

In order to correct these object frames, we simply subtract the extra counts in each well from them, by using the information we obtained from the zero frames. Usually, Tenagra takes three zero frames initially, and then takes a few intermittently throughout the night. These several frames give us a little statistical advantage, as the number of electrons in each well vary from time to time. The more frames there

are, the better the statistical average. The frames taken throughout the night help track the drift in the electronics over time. In IRAF, we statistically combine several zero frames to make an overall average frame, which we then subtract from the object frame. Figure 3.4 shows the comparison between a raw frame and one that has been processed. Notice that the zero subtract has removed most of the gradient from the frame.

Figure 3.2: Zero Frame

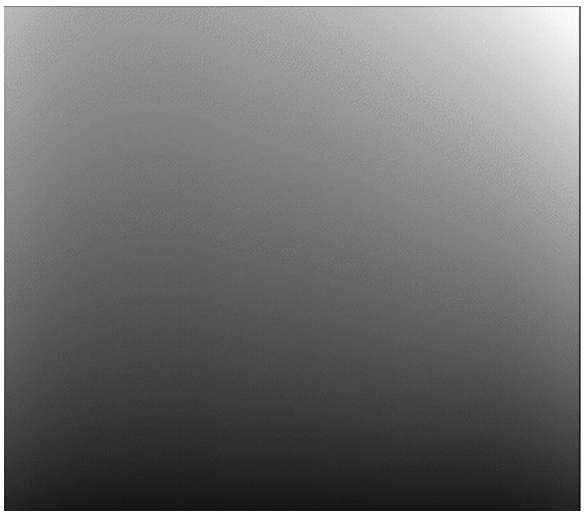

Dark

A dark frame is an CCD image taken with the shutter closed. Because no outside light reaches the CCD chip, the stimulated pixels are due to thermal fluctuations from the running CCD. The amount of what we call "dark current" is linearly related to the exposure time for sufficiently short exposures. Thus, our exposure lengths for the dark frames should be of comparable length as our object exposure.

In order to correct the dark current on the object frames, a similar procedure to the dark correction is followed. Three initial dark frames are taken, and then intermittently throughout the sequence. Using IRAF's darkcombine task, these dark frames are statistically averaged, pixel by pixel, into a master dark frame. Occasionally, stray cosmic rays strike the pixel during the exposure. We correct for this when combining darks by rejecting the two highest and single lowest for every pixel. It also removes the bias level from off the combined frame, since we do not want to be subtracting the bias level twice. This is then subtracted from the object frame. Notice in figure 3.3 the amount of "hot" pixels on the dark frame.

Flat

A flat frame is a CCD image taken of a surface of uniform texture and color. The most common flats are taken of the uniform blue twighlight sky. A flat frame measures the different responses of each individual pixel to the same color and amount of light, which can vary as much to 10 % in a pixel (). Most CCDs are extremely varied in the response of their pixels, Often flat fields show a distinct pattern that identifies the CCD, comparable to a fingerprint. Flat fielding also corrects for vignetting from the imperfections of the optics.

The flat correction procedure is slightly different from the bias and dark corrections. First of all, a different flat frame is taken for each filter and only flat frames are applied to object frames of a corresponding filter. Using IRAFs flatcombine task averages a few flat frames to make one master flat frame. The zero and dark frames are subtracted off the flat frame, as usual. Then the flat frame is not subtracted from the object frame, but rather divided into the frame. Thus, the flat frame "flattens" out the object frame, by weighting each individual pixel according to its sensitivity to light. In other words, the more sensitive pixels are made darker and the less sensitive amplified. Figure 3.3 shows a typical Tenagra flat frame. Notice the donut rings and blemishes in the frame.

Figure 3.3: Dark and Flat Frame

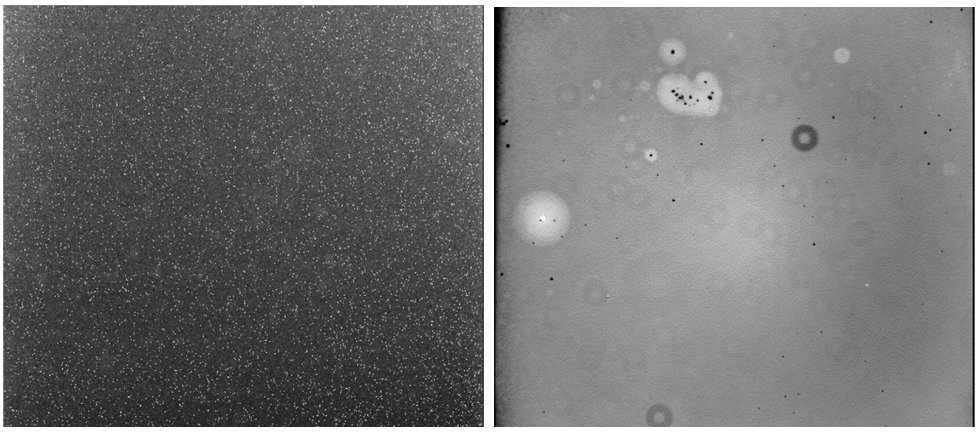

3.1.3 Processed Frames

Here in figure 3.4 we have a comparison between the raw and processed frames for M81. Notice the smooth gradient, the removal of the hot pixels, and the removal of the donuts.

3.2 Photometry

3.2.1 Aperture Photometry

The most basic form of photometry is aperture photometry. On a reduced frame, we place an aperture of a certain radius around our object, whether it be star or galaxy nucleus. The aperture then counts all the electrons in each of the pixels in the area around that aperture. If it included a fraction of a pixel, it would count the same fraction of the electrons in that pixel. The pixel counts are then corrected by subtracting background light (from moon, lights, etc.), and divided by the integration time to obtain a flux. This flux is then converted to a magnitude with the definition

$$m = -2.5 \log F \tag{3.1}$$

Figure 3.4: The difference between a raw and reduced frame

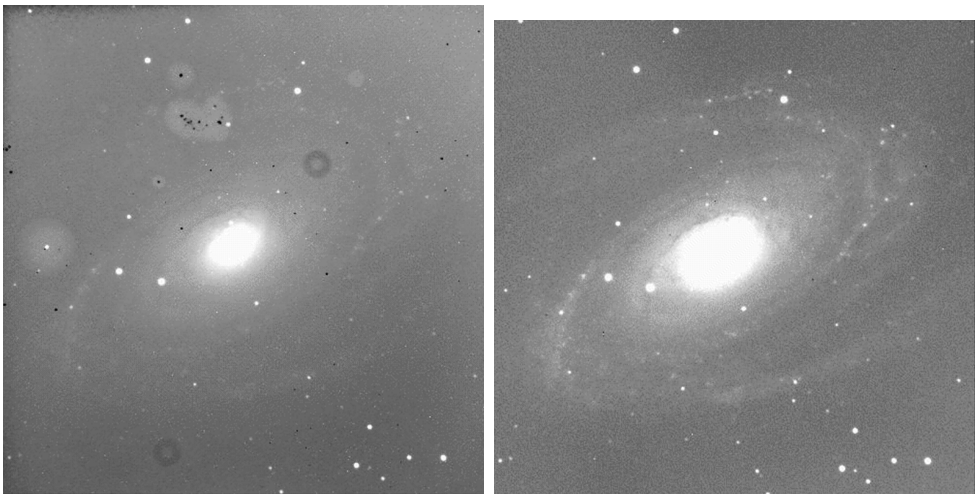

Figure 3.5 shows the stars selected for photometry in M101 and M81.

3.2.2 PSF Fitting

For M101 in the V filter, we also used an IRAF package known as DAOphot, which increases the accuracy of photometry by fitting the image to a point spread function. This fits a gaussian point spread function to several stars in the frame, and then calculates a general trend for the entire frame, and removes this from the image. This better treats the objects in the frame as point sources, which is a better approximation, rather than extended images.

Figure 3.5: The stars selected for aperture photometry in M101 and M81.

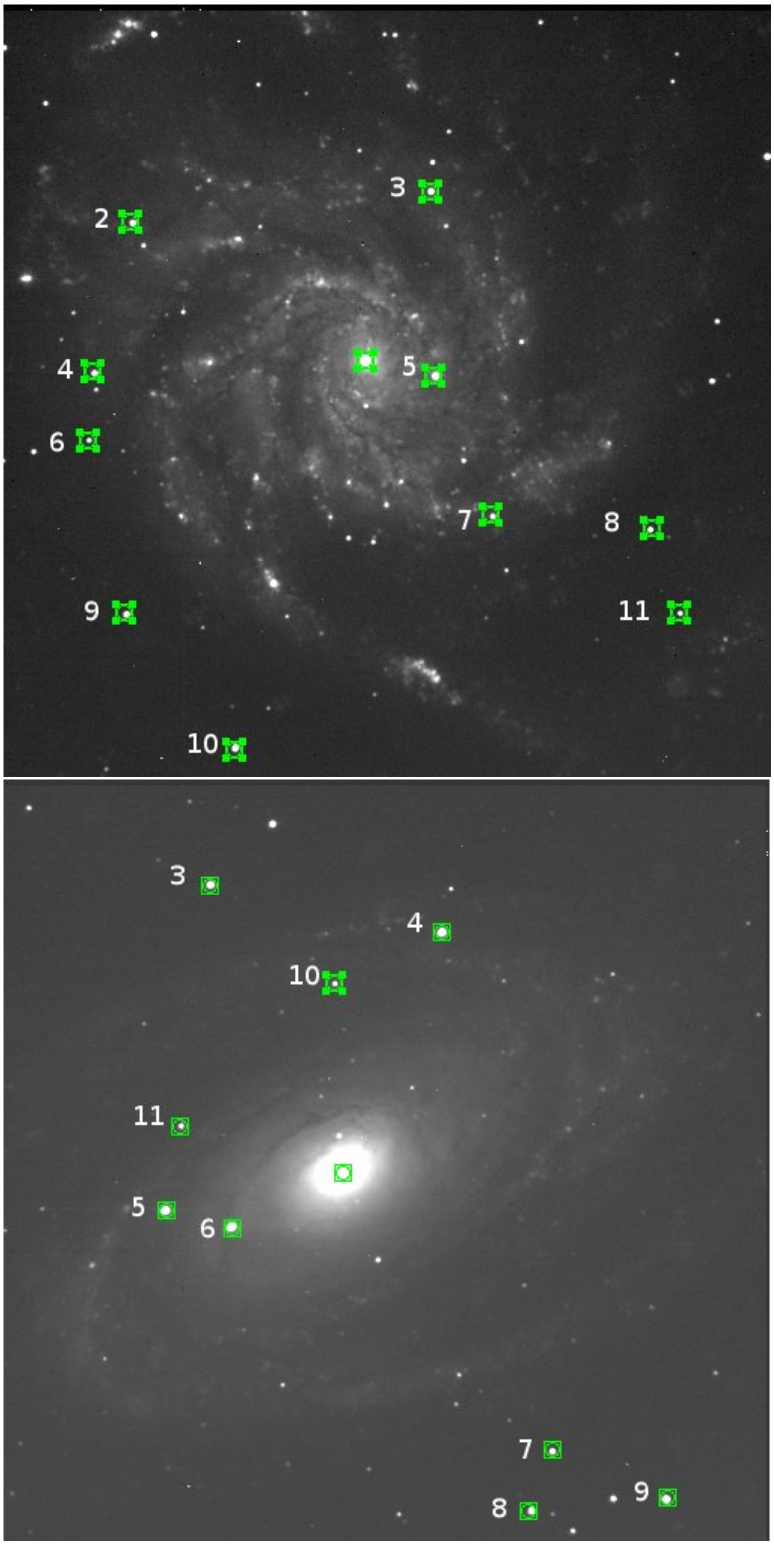

Chapter 4

Analysis

Aperture photometry was performed on the nucleus of M101 an M81, as well as several foreground stars in the field. Two aperture sizes where selected, one at the full width at half maximum (3 pixel radius or 2.61″), and one where the starlight fades into the background noise (6 pixel radius or 5.22″). Photometry was done in the B, V, and R filters. A list of star IDs with their corresponding observation time and magnitude were exported into a spreadsheet. The observation error was determined by the equation

$$\sigma = \sqrt{\overline{x^2} - \overline{x}^2} \tag{4.1}$$

Variation in seeing conditions over time change the apparent size of the star disks. This being the case, the same aperture size would yield different star fluxes, because for each night, either more or less of the star will be included in the same area. As the magnitudes of the stars are plotted over time, much of the variation in the light curve is due to the seeing, rather than any physical processes. We can note in fig 4.1 for M101 that the field stars and nucleus all have the same general curve shape.

The observation error for each star was calculated. The most stable star (i.e. the star with the least deviation from its mean) was used as a correction star. A differential magnitude for the nucleus and each star were obtained by subtracting the magnitude of the correction star from each of the other sources. This removed the general trend caused by the seeing. The error per observation was calculated again for the stars, and a few light curves of the stars with the lowest error and differential magnitudes close to the nucleus (for better comparison) are plotted with the nucleus.

4.1 M101

As shown in the second half of figure 4.1, the nucleus of M101 in the V filter varies much more than the foreground stars. The best results were generally obtained with the 3 pixel aperture. It varies on an order of $\Delta m_V = 0.236$. The most stable star is star 4, which is stable down to 4.7 thousandths of a magnitude (fig A.3), but the average deviation is $\sigma_V = 0.018$.

We also tried removing the general point spread function from M101 in the V filter, in order to get more accurate results. We noticed from analysis on the photometry (see fig 4.2) that the stars were generally more stable than when aperture photometry was used. This method could prove to be more useful and accurate than the standard aperture photometry. Here, the nuclear variation is $\Delta m_V = 1.05$, much greater than the value for the aperture photometry. The most stable stars are only stable down to 6.2 thousandths of a magnitude, but the average deviation is much less at $\sigma_V = .00915$.

The variation in the B and R filters and the 6 pixel radius apertures were in general lower than that of the V with $\Delta m_B = 0.384$ and $\Delta m_R = 0.446$ for the nucleus. The errors per observation in the stars were $\sigma_B = 0.0238$ and $\sigma_R = 0.0194$. These lightcurves can be found in the appendix. Figure 4.3 shows the field of M101 and the comparison of the nucleus size.

4.2 M81

We followed the same analysis procedure in all the filters of M81 as in M101. Figure 4.4 shows the light curve for M81 in the V filter at a 3 pixel ($2.61''$) aperture. The best results were generally obtained with the 3 pixel aperture. The nucleus has a variability of $\Delta m_V = 0.439$ The stars have an average stability of $\sigma_V = 0.0281$. The stars in the B filter were more stable, with $\sigma_B = 0.0139$ but a $\Delta m_B = 0.027$. These figures are not at an aperture of 3 pixels but rather 6. There is no data available for M81 B at a radius of 3 pixels.

We also tried removing the general point spread function from M81 in the B filter, as we had previously. We noticed that the nucleus for the later dates varied significantly from the general trend (figure 4.5), which was unexpected. The results are somewhat difficult to accept, especially the magnitude variation. Here, the nuclear variation is $\Delta m_B = 0.708$, much greater than the value for the aperture photometry. The most stable star is stable down to 6 thousandths of a magnitude, but the average deviation is greater than the aperture photometry at $\sigma_B = .0387$.

The variation in the R filter and the 6 pixel radius apertures were in general lower than that of the V with $\Delta m_R = 0.373$ for the nucleus. The errors per observation in the stars were $\sigma_R = 0.0434$. These lightcurves can be found in the appendix. Figure 4.6 shows the field of M81 and the comparison of the nucleus size.

Figure 4.1: The M101V light curve before and after correction for aperture photometry.

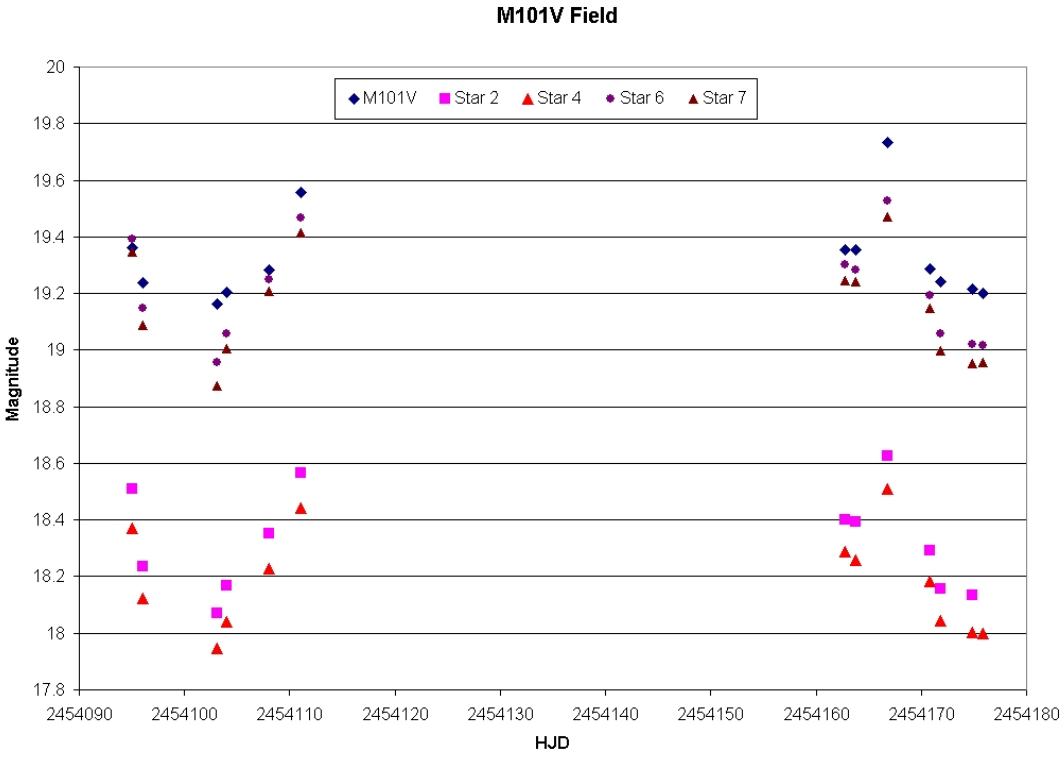

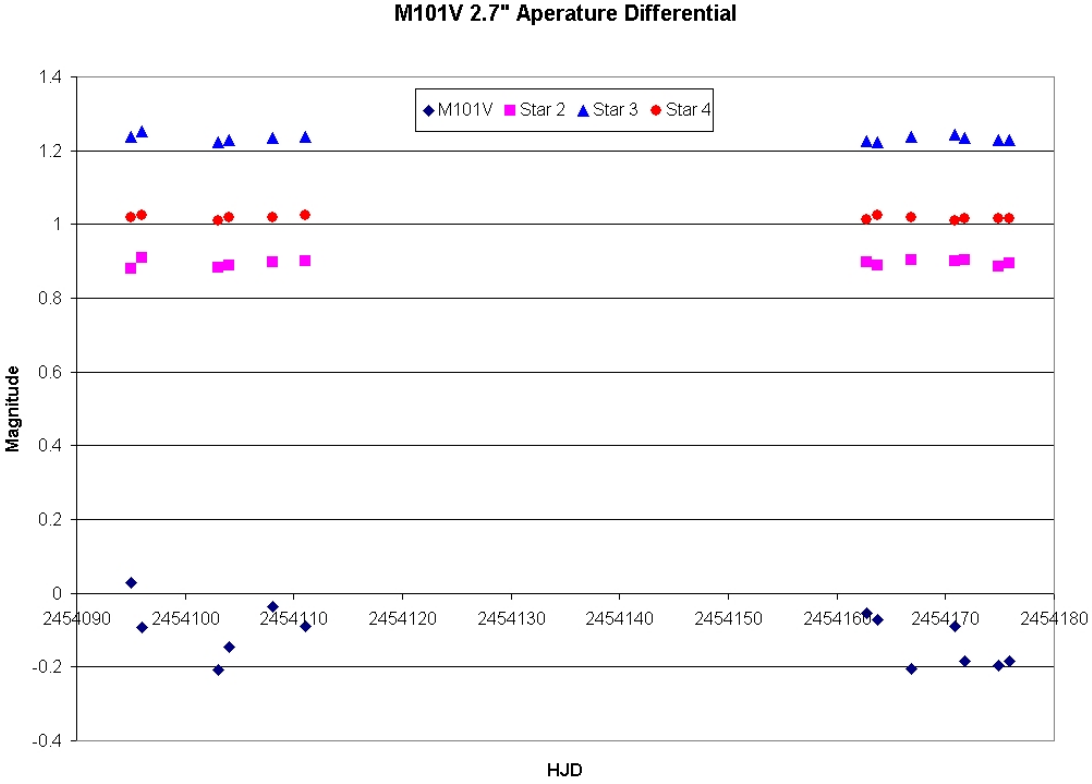

Figure 4.2: The M101V light curve before and after correction for PSF fitting.

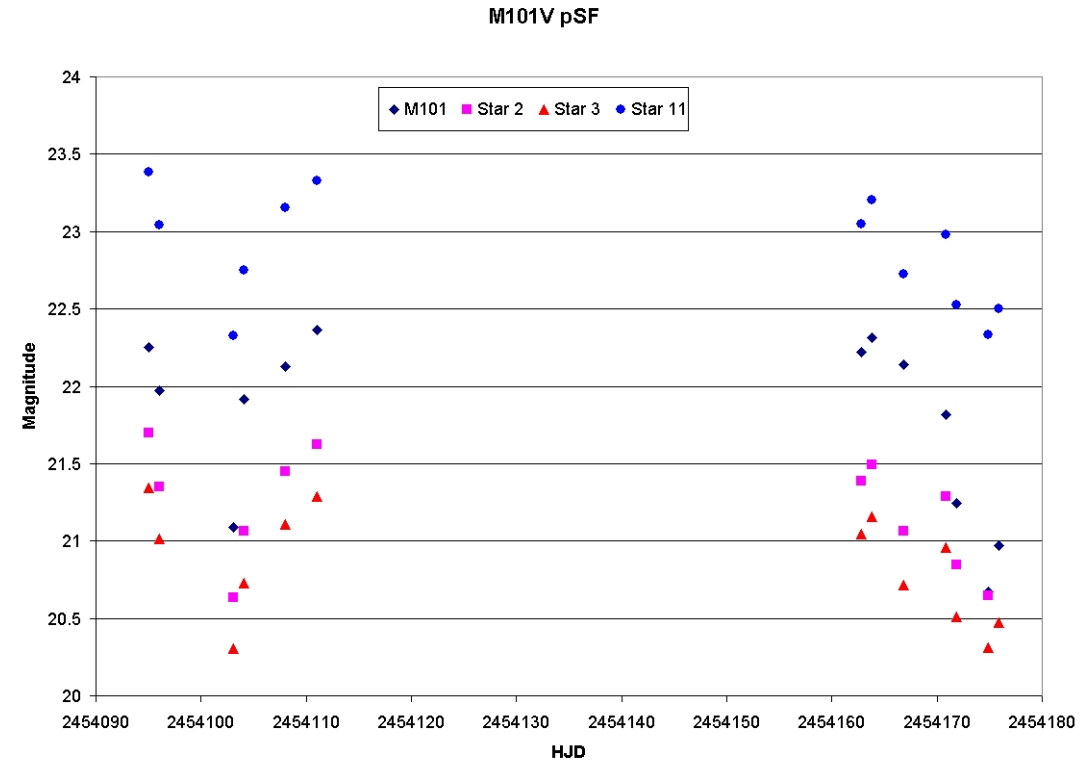

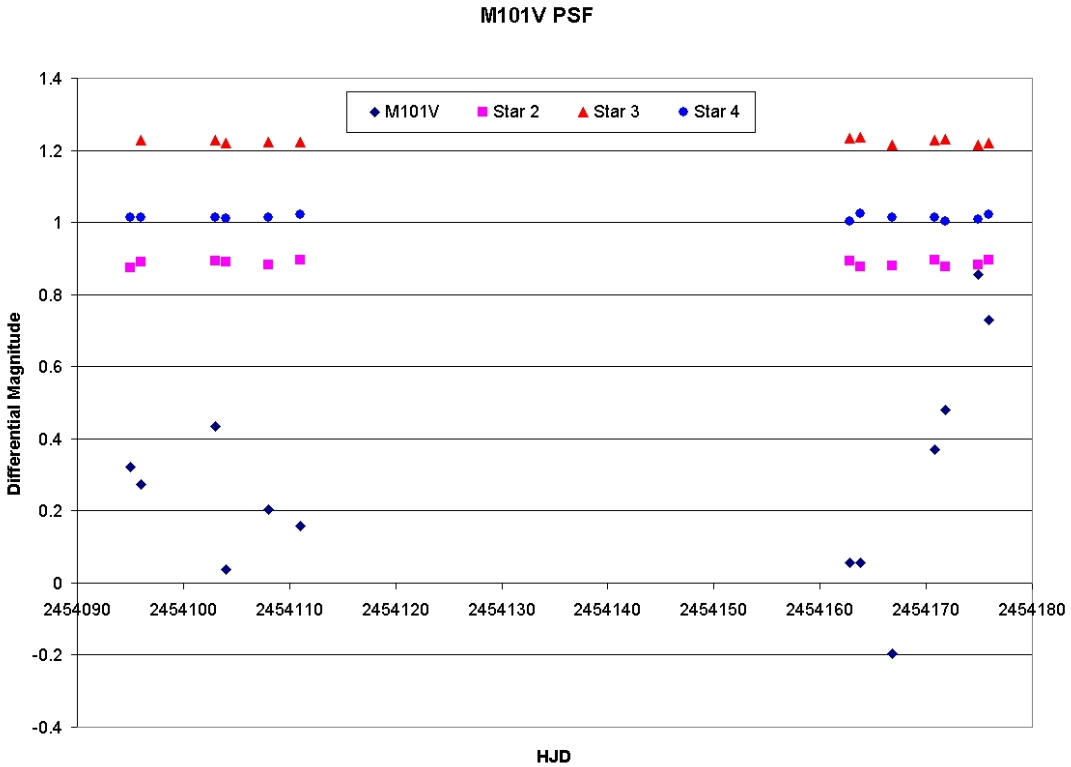

Figure 4.3: The normal galaxy M101 and the field containing the foreground stars. Note the size of the nucleus.

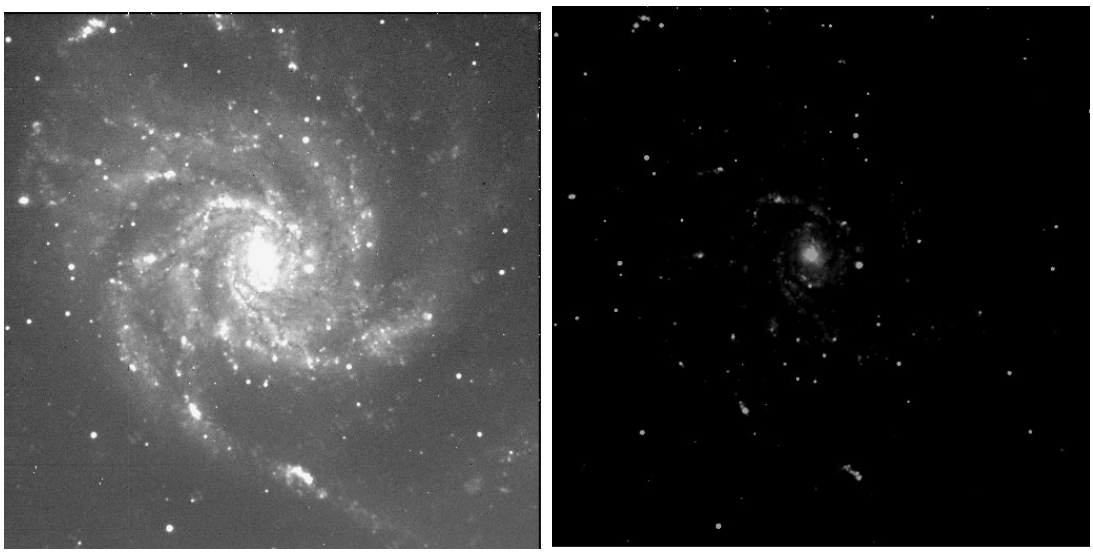

Figure 4.4: The M81V light curve after correction for aperture photometry.

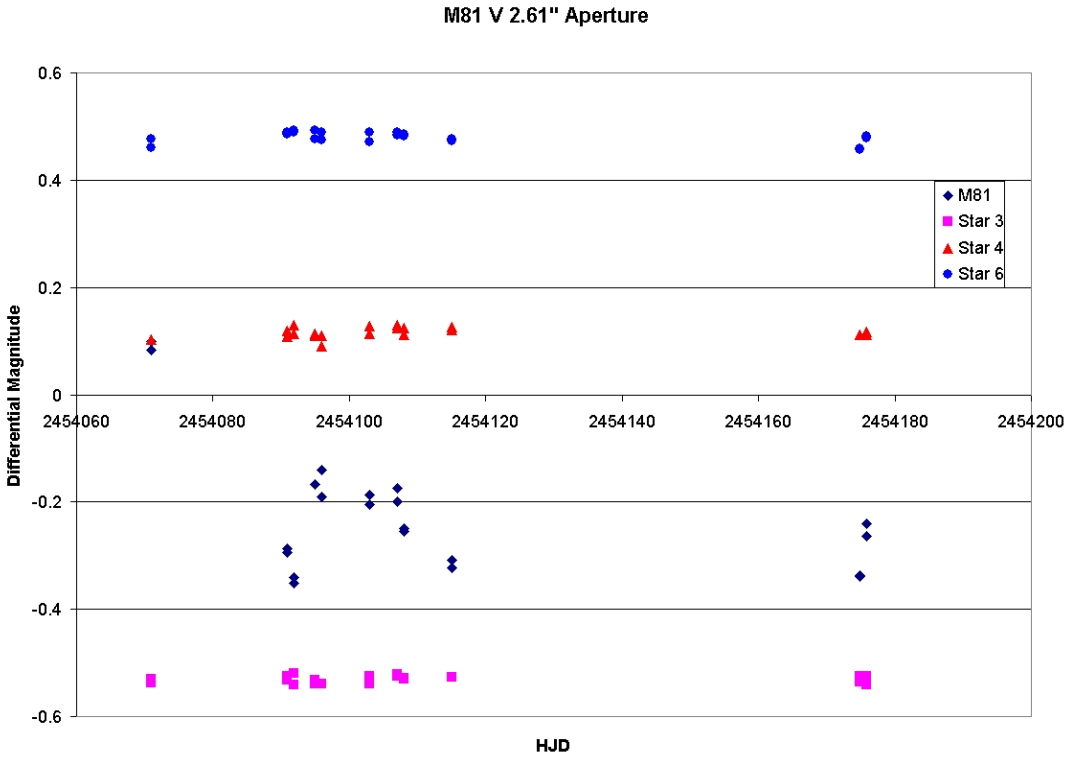

Figure 4.5: The M81B light curve before and after correction for PSF fitting.

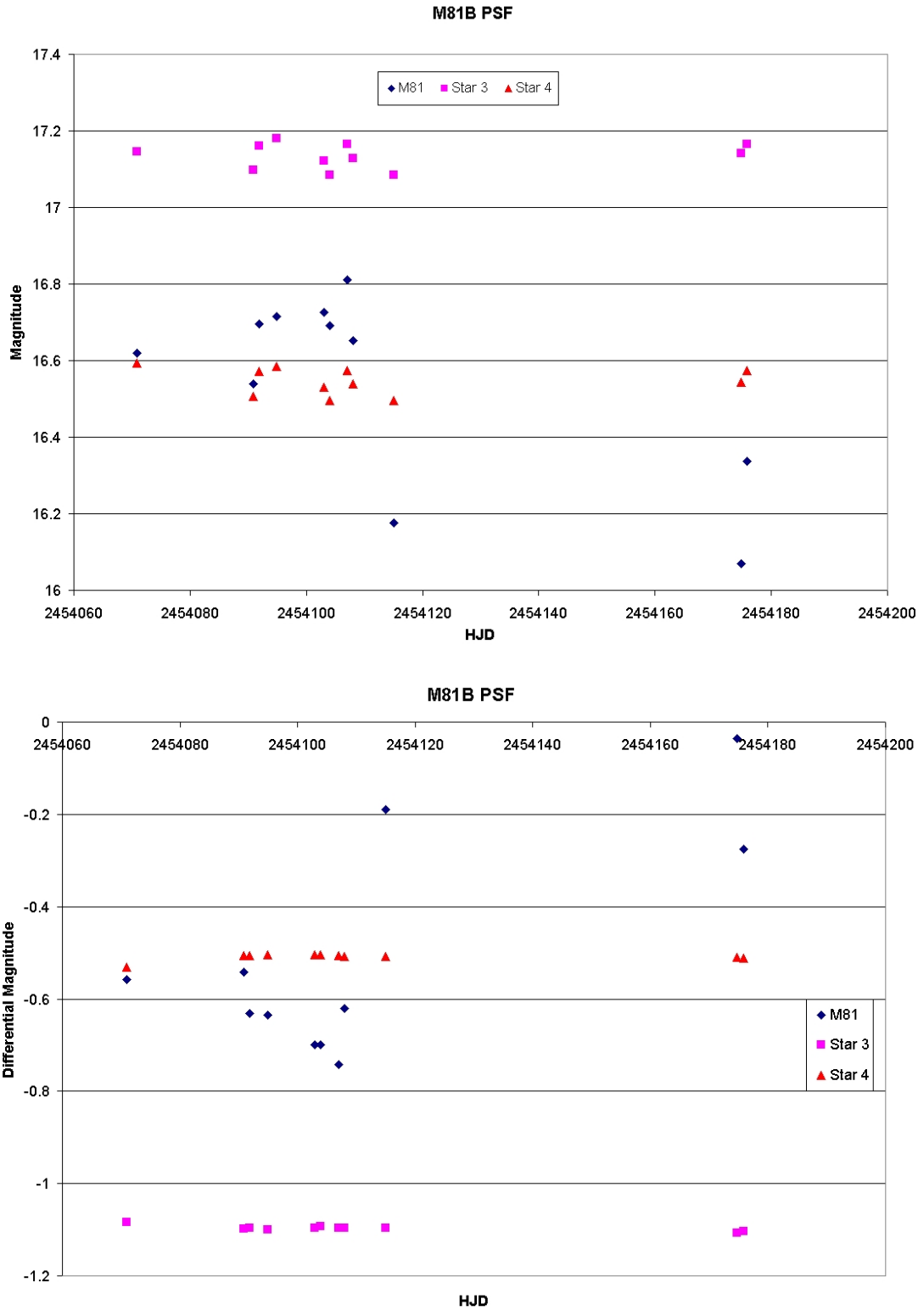

Figure 4.6: The LINER galaxy M81 and the field containing the foreground stars. Note the size of the nucleus.

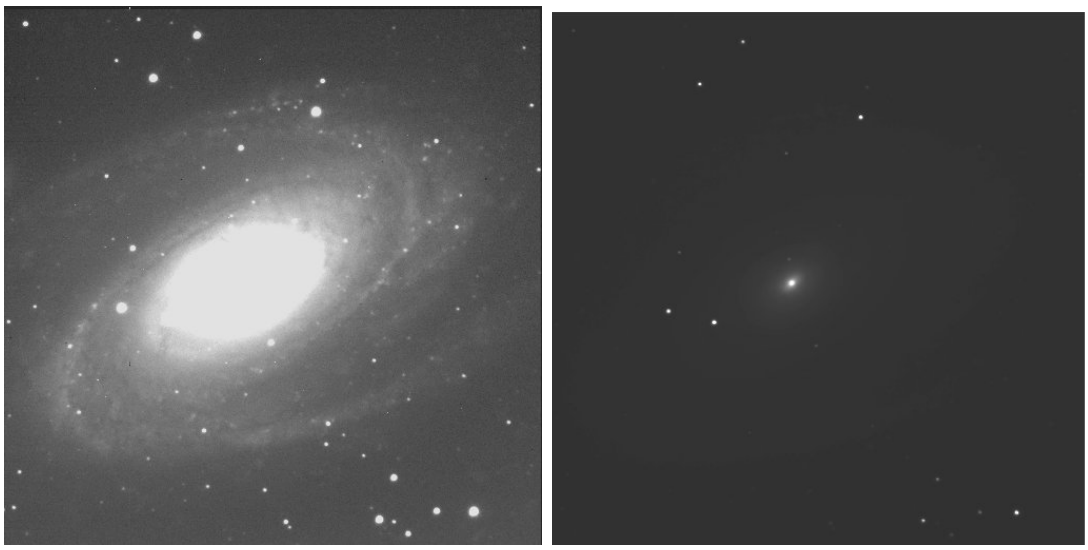

Chapter 5

Conclusion

Aperture photometry on M101 in the V filter varies in the nucleus with $\Delta m_V = 0.236$ with $\sigma_V = 0.018$. The B and R filters show some variation, but to a lower degree. The PSF fitting gave better results, with $\Delta m_V = 1.05$ and a $\sigma_V = 0.00915$.

M81 varies more in the nucleus in comparison with M101 with $\Delta m_V = 0.439$ but only with $\sigma_V = 0.0281$. The B and R filters also show variation, but to a lower degree. The PSF fitting of M81 seemed to fail in its accuracy. Further tests should be done to see if this anomaly could be resolved.

We have shown in the table in A.3 the errors per observation of particular stars in the field that were used as standards. We have also demonstrated the potential use of using PSF fitting in order to obtain more accurate results.

Most essentially, we have begun to collect data on these galaxies in order to set up a baseline for long-term monitoring. We hope that future studies and continued observation over the span of 10-15 years will find periodicity in the variation of these nuclei. We also expect further studies to yield greater accuracy to these results. Ideally, the method of comparison to the galactic bulge profile will be developed and that will become the standard method for nuclear study. These results will increase our knowledge of galactic evolution, and give us a way to test our physical models of black holes.

Appendix A

Light Curves

A.1 M101 and M81

Figure A.1: Light curve of the nucleus and certain foreground stars of M101 at an aperture of 3 pixels in the B filter.

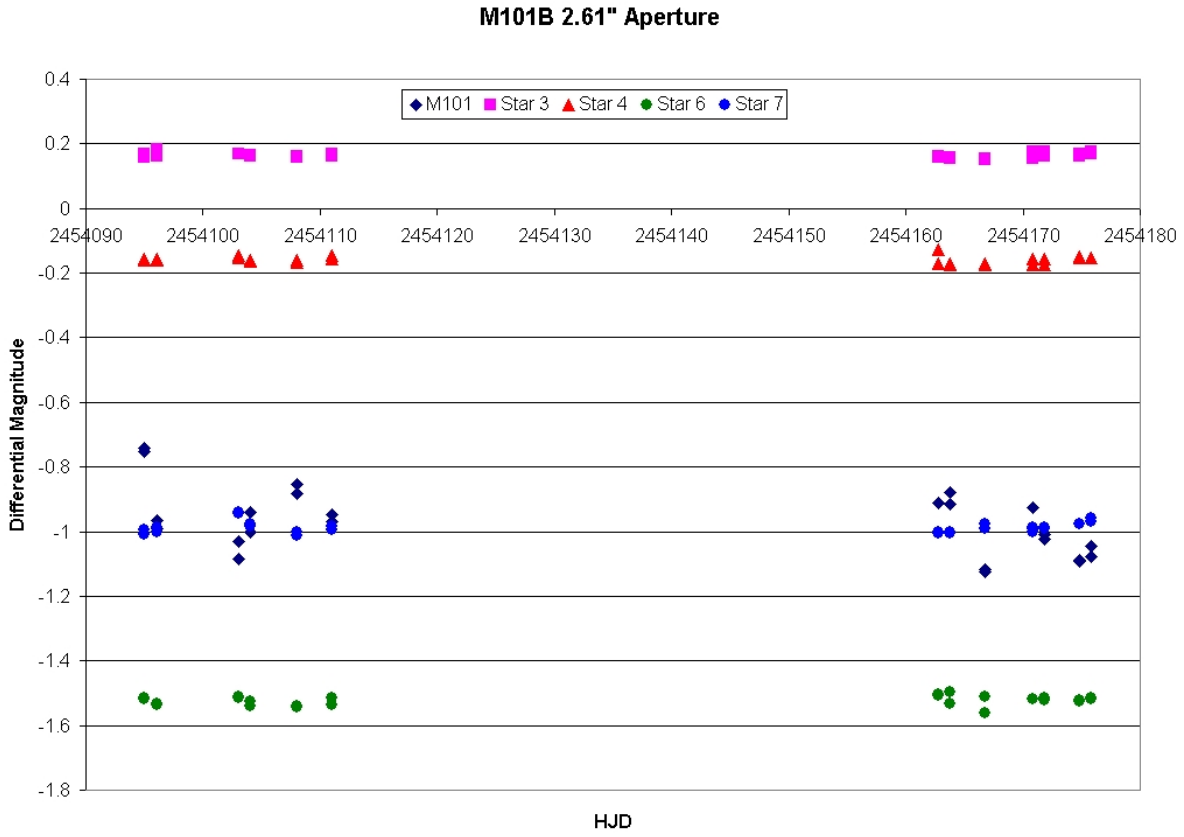

Figure A.2: Light curve of the nucleus and certain foreground stars of M101 at an aperture of 6 pixels in the B filter.

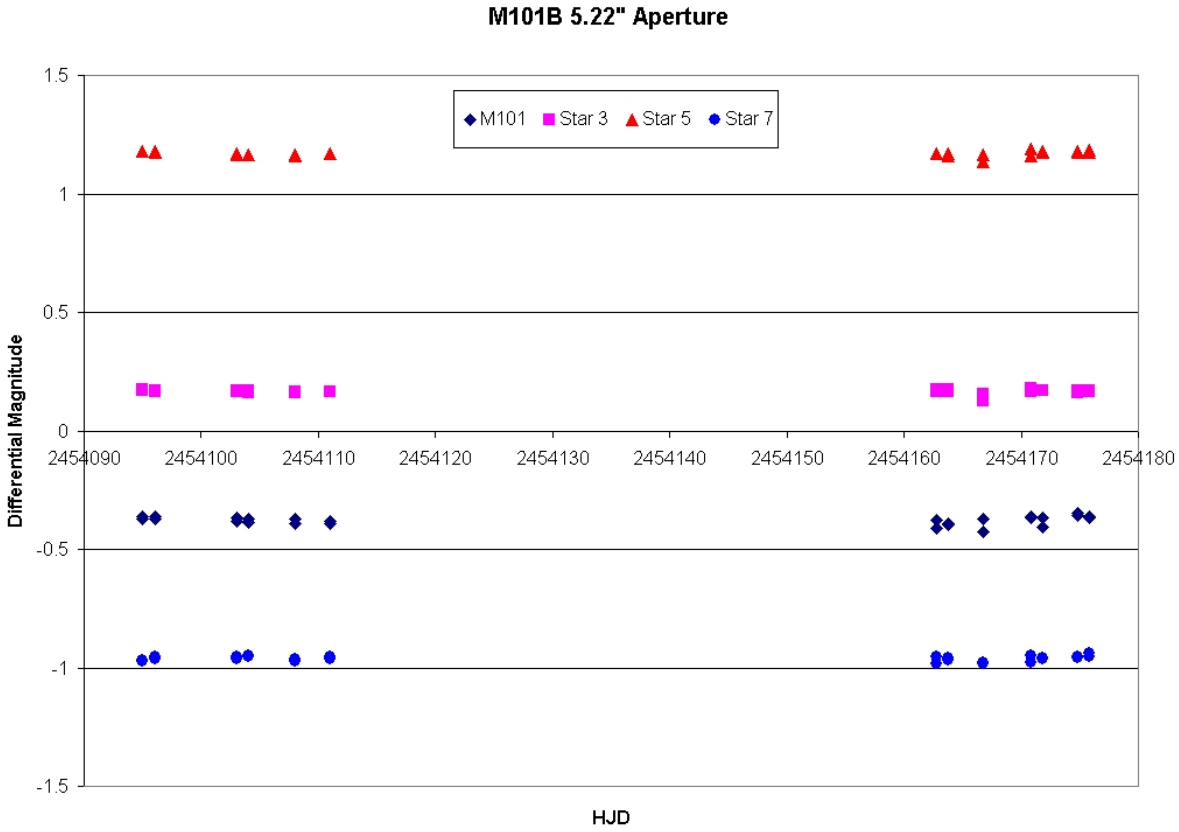

Figure A.3: Light curves of the nucleus and certain foreground stars of M101 at apertures of 3 pixels and 6 pixels in the R filter.

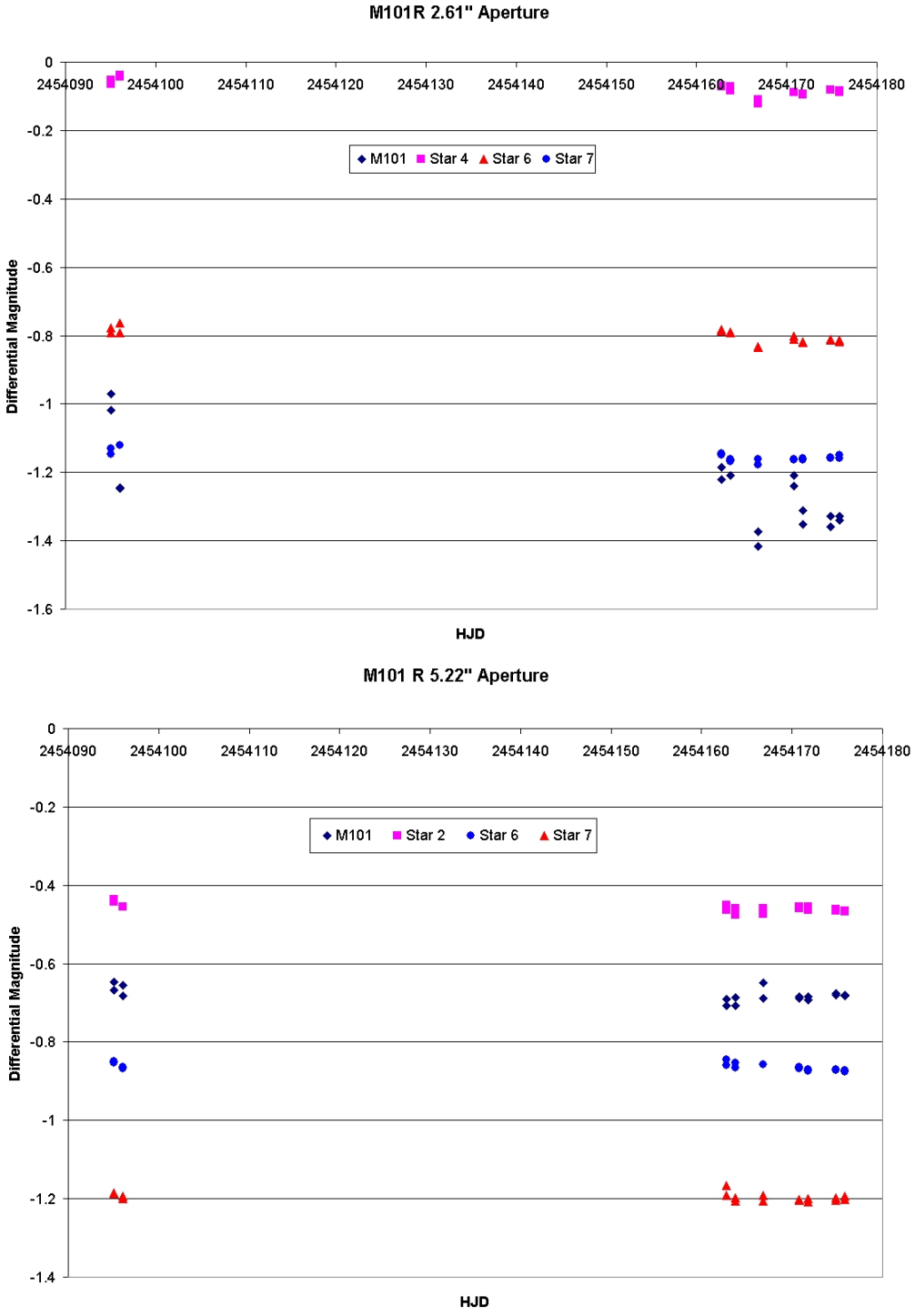

Figure A.4: Light curve of the nucleus and certain foreground stars of M81 at aperture 6 pixels in the B filter.

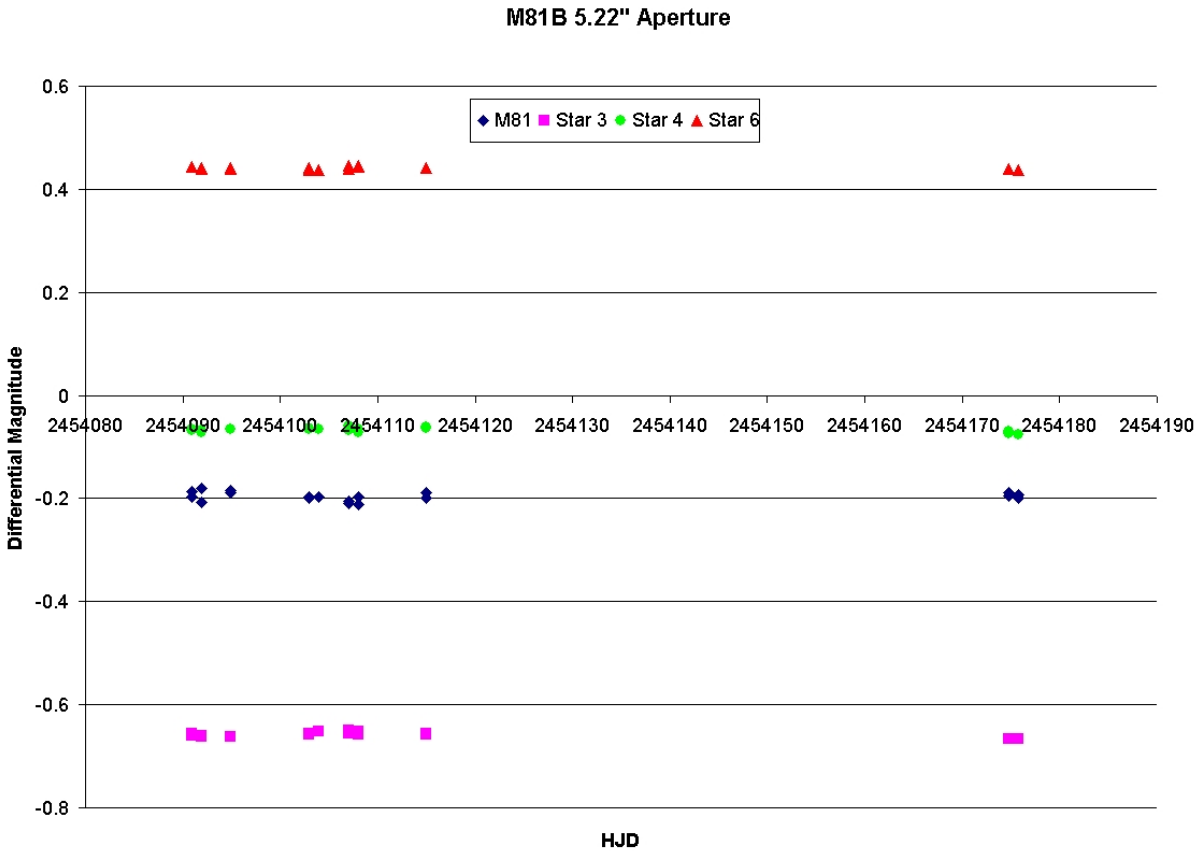

Figure A.5: Light curves of the nucleus and certain foreground stars of M81 at apertures of 3 pixels and 6 pixels in the R filter.

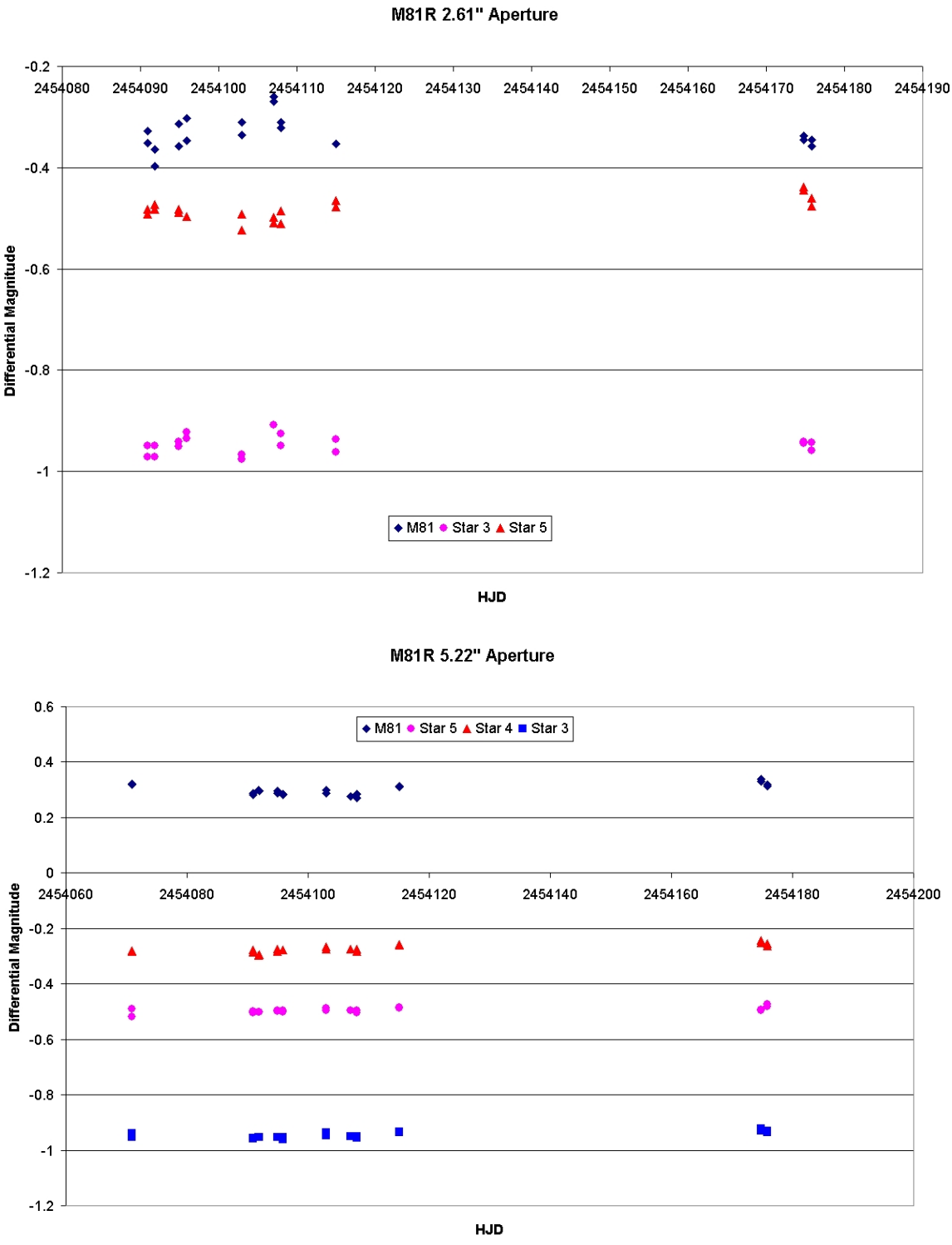

Appendix B

Star Data

B.1 Observation Errors

This table shows the errors for each star in the V filters of M101 and M81.

Galaxy	Star	σ	Galaxy	Star	σ
M101V	2	0.0087	M81V	3	0.0069
	3	0.0082		4	0.0099
	4	0.0047		6	0.0111
	5	0.0112		7	0.0438
	7	0.0113		8	0.0512
	8	0.0323		9	0.0698
	9	0.0150		10	0.0114
	10	0.0285		11	0.0210
	11	0.0467			

References

Carroll, B., & Ostlie, D., 1996, *Introduction to Modern Astrophysics*, Addison-Wesley

Freedman, R.A., & Kaufmann III, W.J., 2005, *Universe, 7ed.*, W. H. Freeman and Company

Massey, P., & Jacoby, G.H., 1992 ASP, 23, 245

McNeil, S., 2004, Thesis(PHD), Brigham Young University

Schwartz, M. 2007, *www.tenagraobservatories.com*

Sterken, C. 1995, IAUS, 167, 134

Van der Marel, R.P., 1999, IAUS, 186, 333